A Prototype DSN X-S Band Feed: DSS 13 Application Status (Second Report)

W. F. Williams
Radio Frequency and Microwave Subsystems Section

This article, the second in a series discussing a new prototype X-S band horn feed for future use at various DSN sites, deals with the combiner which was designed and fabricated for injecting X- and S-band into the horn. It also discusses predicted performance at DSS 13 by the calculated scattering of the model radiation patterns from the DSS 13 hyperbola.

The results indicate that the present version of the S-band combiner is much too narrow for use in both receiving and transmitting and that the horn patterns, when scattered, yield an improved efficiency over the present horn-hyperbola system.

I. Introduction

The first status report (Ref. 1) of this series discusses the design of a dual-band (X-S) corrugated horn for DSN applications. A half-scale model of the design was fabricated and measured. It fulfilled the requirements of the X-S feed horn program. The radiation patterns and efficiencies of this horn were presented in Ref. 1.

Since this horn is to perform at both X- and S-band simultaneously, a diplexer or X-S combiner must be developed which can inject these signals into the horn. The most important requirement or characteristic of this combiner is that it does not contribute any significant additional loss to the X-band signal. A 0.02-dB X-band loss in this combiner would add 1.4 kelvin to the system noise temperature and this amount is significant in DSN low noise systems. Therefore, it was concluded that the combiner should add less than 0.02 dB to any existing losses in the presently used horn at X-band.

A design technique for satisfying such a difficult requirement was provided by a consultant to JPL (S. B. Cohn, Seymour Cohn Associates, Encino, Calif.). This technique consists of an outer radial waveguide line concentric with the horn and terminating (at the line inner radius) in the horn. The radial line has two circumferential slot chokes to reject any X-band passage. The outer radius of the radial line is excited with the S-band signal, which then passes through and into the X-S feed horn. The theory is discussed in Section II. This technique was used in a full-scale design and the combiner was fabricated. The combiner performed very well at X-band; loss or additional noise from the unit was immeasurably low. However, it suffers from being extremely narrowband in the S-band. The bandwidth (about 50 MHz) is only

sufficient for one function, and in this case the receiving function (2.295 GHz) is chosen. Future additional work will be directed toward increasing the bandwidth to encompass the transmit band also. The final design is discussed in Section III.

A half-scale model of this combiner was fabricated and used with the half-scale model X-S horn (Ref. 1). S-band pattern measurements indicated that the horn was satisfactorily excited through the combiner. X-band was also unaffected.

It then remained to theoretically scatter these measured horn patterns from a computer model of the Venus site (DSS 13) subreflector. This subreflector is a 96-inch (243.84 cm) diameter hyperboloid, whose central region (25.4 cm diameter) is cone shaped, acting as a vertex plate. The hyperboloid is surrounded by a circumferential flange which deflects most of the forward spillover back into the main paraboloid. This flange is about 30.48 cm wide, making the total subreflector 120 inches (304.8 cm) in diameter. A JPL symmetrical scattering computer program was used to calculate the scattering of the horn patterns from the subreflector at selected frequencies in S-band and X-band. This theoretical scattering is discussed in Section IV.

II. The Combiner

The general specifications that were used to define an X-S combiner are as follows:

Frequency

2.1 to 2.3 GHz at S-band (9.09%)
8.4 to 8.55 GHz at X-band (1.77%)

Output Polarization

RCP at S-band
RCP and LCP simultaneous at X-band

Losses

S-band, < 0.2 dB
X-band, < 0.02 dB (relative to horn without combiner)

Power

S-band, 20 kW CW
X-band, receive only

Growth Potential

S-band from 2.1 to 2.4 GHz at 200 kW CW
X-band from 7.1 to 8.55 GHz with 200 kW CW at 7.1 GHz

The technique chosen for this combiner is to feed the S-band into the horn through a circumferential slot that is designed to stop the X-band with a choke or band stop filter. This is illustrated in Fig. 1. The radial line injection region is shown within the horn proper at a position to obtain good impedance matching. The dimension b' is chosen at less than one-half wavelength at the highest X-band frequency. This limits any attempts at X-band propagation within the line to TM^r_{m0} radial modes, where m = number of $\lambda/2$ variations around the circumference, and there are no $\lambda/2$ variations in b' direction. The TE^r_{20} (m=2) radial mode is excited by the X-band HE_{11} wave. Therefore, the radial line band stop filter is designed to stop X-band in the TE^r_{20} radial line mode, and also to present a short circuit looking into the annular opening at X-band. This will result in negligible effect on the X-band HE_{11} wave, i.e., negligible leakage, reflection, or mode conversion.

The S-band signals S_1 and S_2 are fed inward with 180-deg phase difference to yield the horizontal HE_{11} S-band wave in the conical horn, and similarly with S_3 and S_4 for vertical HE_{11} polarization. Waveguide T-hybrids are used, for example, to achieve the equal amplitude, 180-deg power splits and a waveguide 3-dB quadrature coupler to excite these T hybrids. Then one input will yield RCP and the other LCP at S-band.

The design of the X-band choke slots is illustrated in Fig. 2. Dimension b of Fig. 2(a) is chosen at 0.35 in., about 1/4 a guide wavelength in X-band. Using handbook formulas (Ref. 2) the remaining dimensions for the choke are obtained and are indicated in Fig. 2(b). A second choke was added according to the dimensions of 2(c). Beyond these X-band chokes, the radial line continues for a short distance, and is then terminated in four places with step junction transformers. These transformers have four steps and terminate in standard WR430 waveguide.

A photograph of this combiner is shown in Fig. 3. The unit has been separated into two sections for viewing. The section on the right is the input side, showing the taper to a small X-band input end. On the left is the section with the pair of X-band chokes. The addition of four plugs in the second choke was made to improve matching.

III. Combiner Operation

Figure 4 is a block diagram of the laboratory measurement arrangement used to perform the final design development of the combiner. A unit was constructed to the dimensions of the preceding section and used in this measurement to deter-

mine the final required input transformer design and other final details.

Opposite pairs of S-band inputs (① and ②, Fig. 4) must be measured and developed together since they are used together to create a linear polarization (a HE_{11} circular waveguide mode) and there is significant cross-coupling between them. The other terminals (③ and ④) are decoupled from the first pair and used to create the orthogonal linear mode. The two pairs, taken together, will generate circular polarization. These opposite pairs must be excited in phase opposition, i.e., 180 deg out of phase with each other, in order to properly generate this TE_{11} mode instead of the next higher mode, the TM_{01}.

The S-band test generator is therefore fed into an E-H plane tee (180-deg hybrid). This will immediately develop the 180-deg phase difference when using the E-plane input arm. The arm lengths to the combiner inputs must then be equal in order to maintain this 180-deg phase differential. A slotted line is used to perform the measurement on an input arm, and therefore a straight waveguide section of the same phase length is used in the other input arm to maintain this exact phase relationship. In this manner the mutual coupling between opposite arms is "tuned out" as though part of a mismatch reflection.

It was determined by these measurements that an inductive iris was needed at the waveguide inputs to the combiner. This S-band waveguide is only 0.89 cm (0.35 in.) high and the standard 10.92 cm (4.3 in.) wide. This matched input in narrow waveguide was then transformed up to the standard WR430 size using a 5-step, 4-section, waveguide transformer.

Below are tabulated the final voltage standing wave ratios (VSWR) for this combiner.

Frequency, GHz	VSWR
2.100	9.5
2.150	4.5
2.20	2.685
2.225	2.014
2.250	1.501
2.275	1.237
2.300	1.045
2.325	1.195
2.350	1.54
2.375	2.110
2.400	2.940
2.450	6.2
2.5	16.5

The graph of these numbers is shown in Fig. 5. From this it is noted that the bandwidth is only 100 MHz for a VSWR of less than 1.5. This will be suitable for the receive-only operation; however, another solution must be found for future use of the horn for S-band transmission also.

A final and most important characteristic of the combiner is that it must have extremely low loss at X-band, i.e., that it not contribute any more noise to the system than does the existing 22-dB standard being used at 64- and 34-m stations. This noise was measured by using the combiner and a partial full-scale horn; one being fabricated for final use. The X-band first section, horn input was used with the combiner and a second section of the new horn. This was used with the X-band maser for measuring total noise temperature by comparing it with an identical system using the 22-dB standard X-band horn. The standard horn has a certain measurable noise level when looking to the open sky. The new horn, and combiner, are then substituted to determine a different noise level as caused by this different configuration. A long sequence of these substitution measurements was made. The result of all measurements indicated that essentially no difference existed between the two systems. If some small noise was added by the combiner, then it was cancelled by a slightly lower horn loss. This indicates that when this horn-combiner replaces the present horn-reflex plate, the figure of merit will improve by at least a value equivalent to degradation caused by the reflex plate.

IV. Calculated DSS 13 Performance

Figure 6 depicts the subreflector used on the Venus site antenna, DSS 13. This hyperboloid with vertex plate was originally sized and designed for use with the S-band feed horns typical at the DSN. The outer rim or flange is used to capture energy beyond the normal hyperboloid edge and hence reduce forward spillover. The captured energy is then reflected back into the paraboloid at random phases. The result is a very slight degeneration of phase across the main aperture but a large reduction in rear spillover and hence in noise temperature. The vertex plate, which is a simple conical section in the hyperboloid center, scatters energy away from the center of the paraboloid, thus reducing reflection back into the feed horn and also reducing the amount of energy to be finally blocked by the subreflector. This energy also finds its way onto the main parabola at random phases, thus causing a further slight degeneration of the phase pattern across the main aperture face.

JPL has a computer program (Ref. 3) which calculates the scattered or reflected electric field of an incident field from any symmetric reflective surface. The measured radiation patterns of the X-S band model feed horn were scattered

from the Venus site subreflector using this symmetric scattering program. These resulting scattered patterns are used in a JPL efficiency program to determine the final microwave efficiency of the new X-S feed horn at DSS 13.

Figure 7 is typical of the X-band scattering results. This pattern is obtained by assuming that the half-scale pattern at 17.0 GHz is identical to a full scale pattern of 8.5 GHz. Note the very deep nulls in the shadow region caused by the vertex plate of the subreflector. This shadow area is broader than it needs to be for X-band operation. The vertex plate was developed for S-band use, explaining the less than ideal X-band pattern.

It is interesting to compare this scattering with that of the DSN standard X-band horn scattered from the same subreflector. Figure 8 depicts the result. Note that the null central region (±10 deg) is about the same as Fig. 7. The significant difference is in the middle region, from 30 to 45 deg. Here the energy tapers off somewhat (Fig. 8) while in Fig. 7 a more constant illumination is maintained due to the "squareness" of the new horn pattern at X-band. This will result in a higher illumination efficiency for the new horn.

The following is a tabulation of efficiencies for these two cases:

Efficiency	Frequency = 8.5 GHz	
	22 dB Standard	New X-S Dual Band
Forward spillover	0.9707	0.9897
Rear spillover	0.9968	0.9956
Illumination	0.8019	0.8480
Phase	0.8894	0.9005
Blockage	1.0000	1.0000
Cross-polarization	0.9990	0.9990
Total	0.6894	0.7517

The result is an approximate increase in efficiency of 6%, or about 0.38 dB. Nearly 5% of this is from illumination efficiency (more nearly uniform illumination), while the remainder is from forward spillover and phase. The DSN 22-dB standard horn has some sidelobe energy in the form of shoulders on the main lobe while the new X-S horn is completely free of sidelobe energy. These shoulders represent nearly 2% more spillover than occurs with the new horn.

The S-band pattern of the new horn was also scattered from the Venus site subreflector. Figure 9 depicts this scattering for the new horn at S-band. The 4.6-GHz pattern of the half-scale model is used at 2.3 GHz on the subreflector. Figure 10 depicts the 22-dB standard when scattered at 2.295 GHz. The general shapes of these patterns are much alike. This subreflector with vertex plate was designed to fit the pattern of the 22-dB standard at S-band.

Below is a tabulation of these two S-band pattern efficiencies when scattered from the Venus subreflector.

Efficiency	Frequency = 2.295	
	22-dB standard	New X-S band
Forward spillover	0.9707	0.9420
Rear spillover	0.9943	0.9960
Illumination	0.8654	0.8430
Phase	0.9637	0.9120
Blockage	0.9741	0.9690
Cross-polarization	0.9998	0.9998
Total	0.7839	0.6988

The result for S-band has been a drop in efficiency of 8.5% or about 0.5 dB. The most significant difference is in phase efficiency. This is due in part to the S-band displaced phase center from the X-band phase center in the new X-S horn. It is also due in part to the vertex plate and subreflector flange, which were specifically designed for the S-band 22-dB standard horn, and which result in some phase error, as discussed above.

Forward spillover and illumination are also poorer in the new horn at S-band. An investigation of the radiation patterns (Ref. 1) will indicate the reason.

The very slow falloff of energy beyond the −10 dB level contributes to excessive spillover and the "triangular" shaped beam gives more illumination taper and hence a lower illumination efficiency. If the new X-S horn is made larger (larger aperture at the same flare or cone angle) the S-band performance will slowly improve, approaching X-band performance.

Acknowledgement

The author would like to acknowledge the efforts of Dave Nixon, Harry Reilly, and Jim Withington in this program. They have done a major portion of the work of bringing this task to a successful conclusion.

References

1. Williams, W. F., "A Prototype DSN X-S Band Feed: DSS 13 First Application Status," in *The Deep Space Network Progress Report 42-44,* pp 98-103, Jet Propulsion Laboratory, Pasadena, Calif., Apr. 15, 1978.
2. *Radiation Laboratory Waveguide Handbook,* Vol. 10, pp. 337-350, edited by N. Marcuvitz.
3. Rusch, W. V. T., *Scattering of an Arbitrary Spherical Wave by An Arbitrary Surface of Revolution,* Tech. Report 32-979, Vol. 1, Jet Propulsion Laboratory, Pasadena, Calif., pp. 31-39, April 1967.

Addendum

Since this second report was originally prepared, the full-scale X-S horn has been fabricated and its radiation patterns were measured. Some significant differences were noted from the patterns of the half-scale model discussed in this article. At the upper end of the X-band frequency range, the E and H plane patterns of the new horn were noticeably different from each other and not the near overlays as were those of the half-scale model. It is expected that this is due to some additional hybrid mode generation in the horn because of the combiner input slot or because of the change of flare angle in this slot region.

In any event, these full-scale patterns were scattered from the Venus site subreflector in the manner of the above Section IV with the following results:

	Frequency = 8.5 GHz
Efficiency	New X-S dual band
Forward spillover	0.9670
Rear spillover	0.9958
Illumination	0.8410
Phase	0.8980
Blockage	1.0000
Cross-polarization	0.9920
Total	0.7214

We observe about 3% less in efficiency than anticipated from the half-scale model; 2% of this occurs in forward spillover while the remainder is divided among the other factors. This occurs because one plane (E-plane) is broadened in this upper frequency region and results in the additional forward spillover. The expected 0.38 dB improvement, for this particular version of the new horn, is therefore reduced to 0.2 dB improvement. Effects during subsequent development of this horn may regain the full improvement potential.

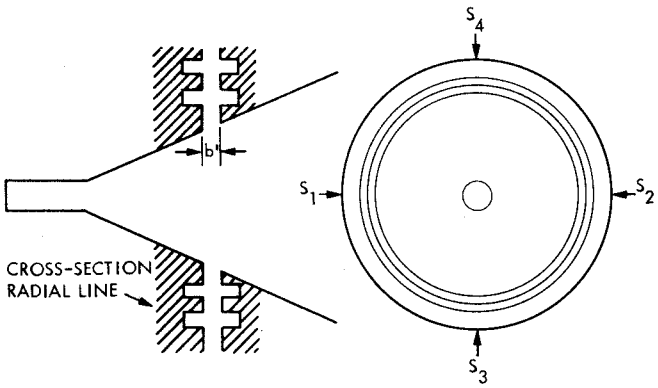

Fig. 1. The combiner concept

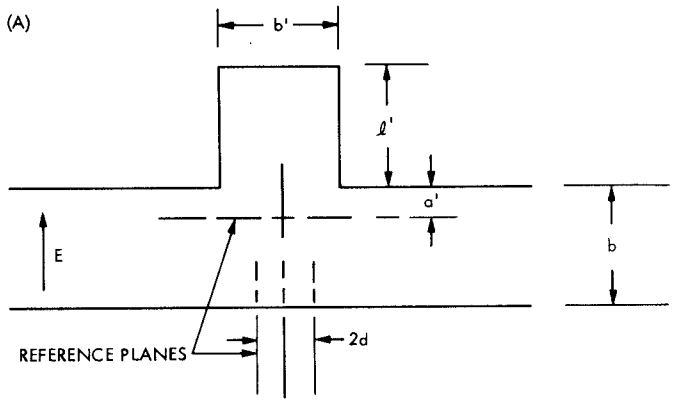

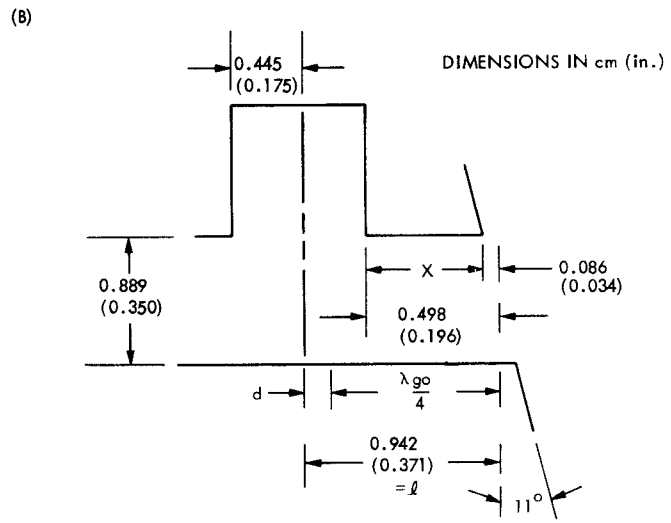

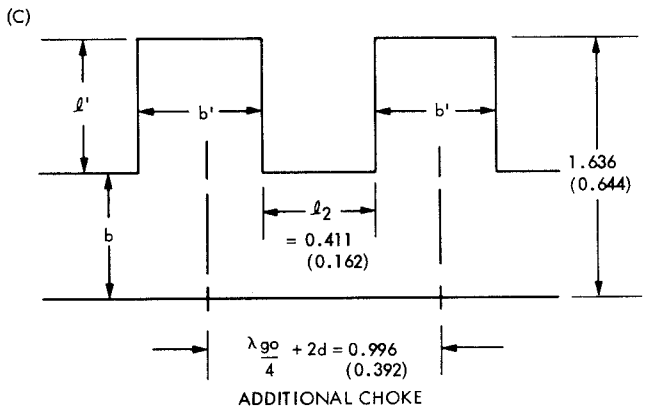

Fig. 2. Choke design

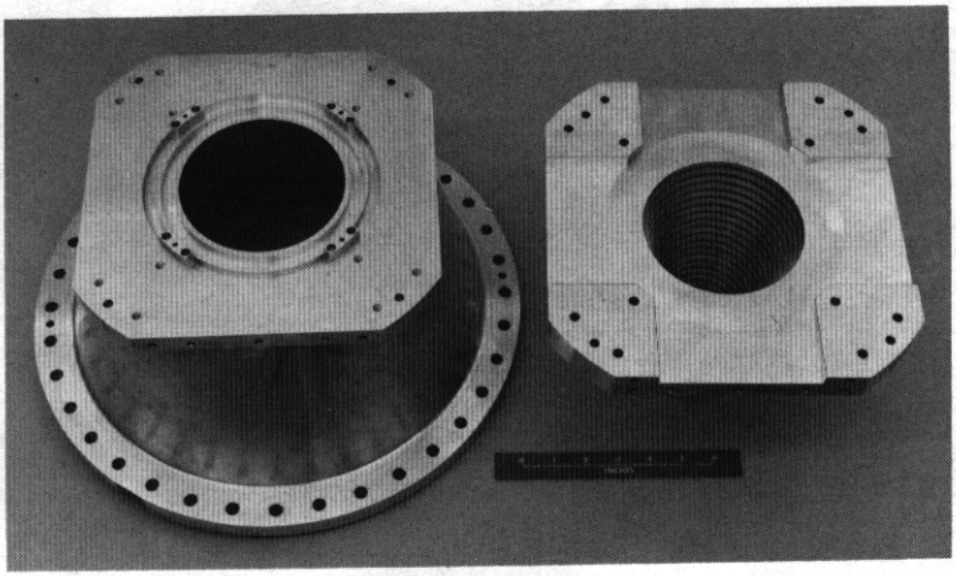

Fig. 3. The combiner

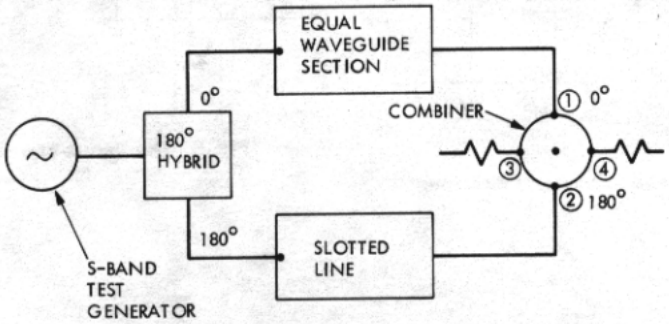

Fig. 4. Laboratory testing setup

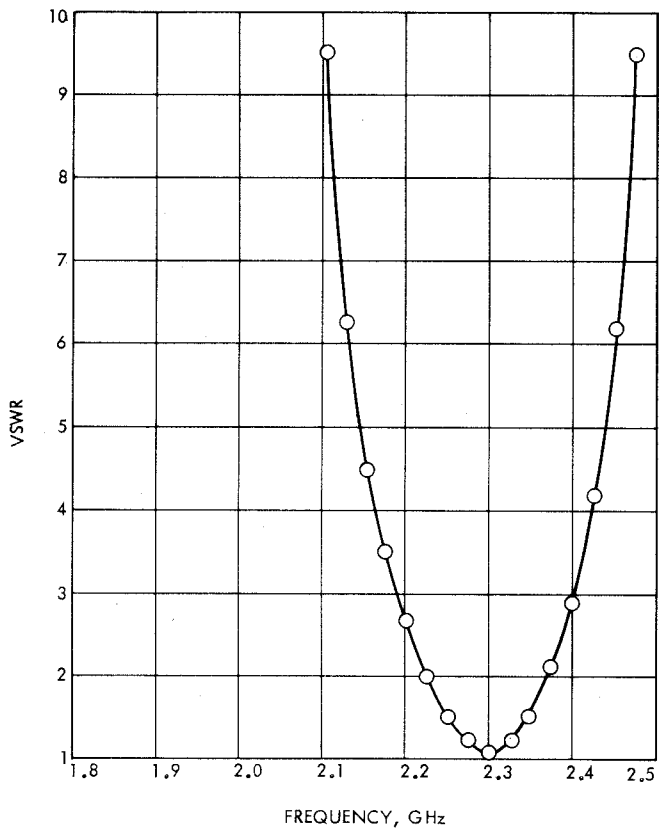

Fig. 5. X-S diplexer S-band slot feed impedance matching

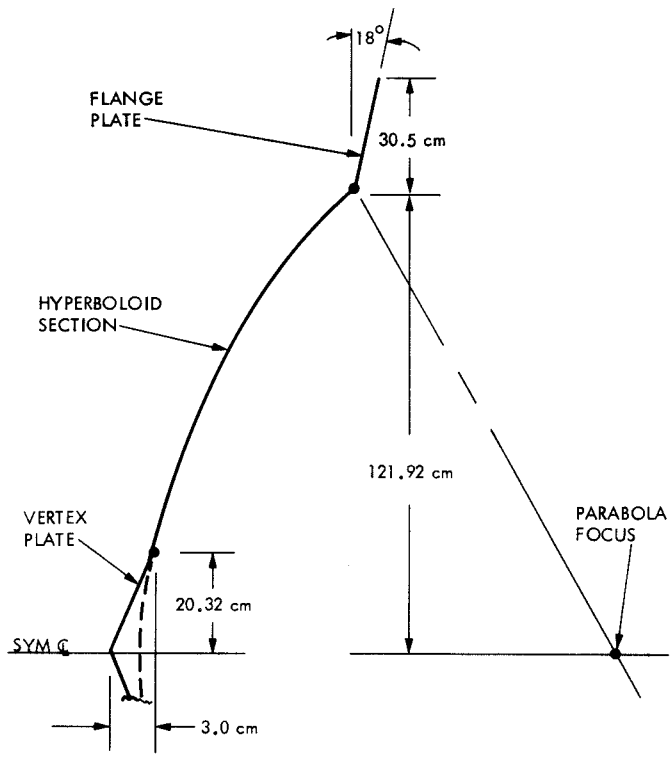

Fig. 6. The Venus site subreflector cross-section

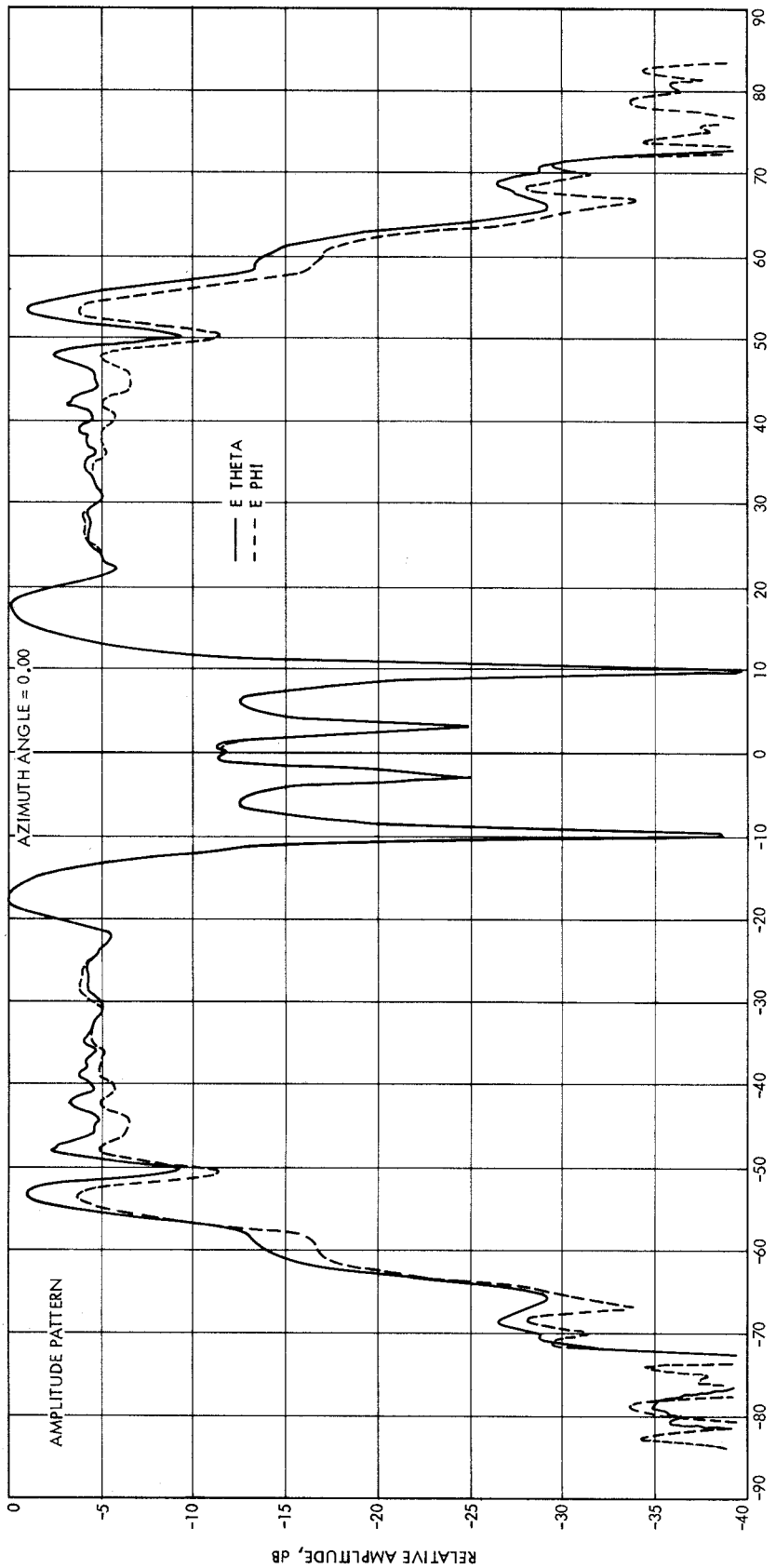

Fig. 7. The 17.1-deg horn at 17.0 (8.5) GHz; Venus site hyperboloid with flange and vertex plate

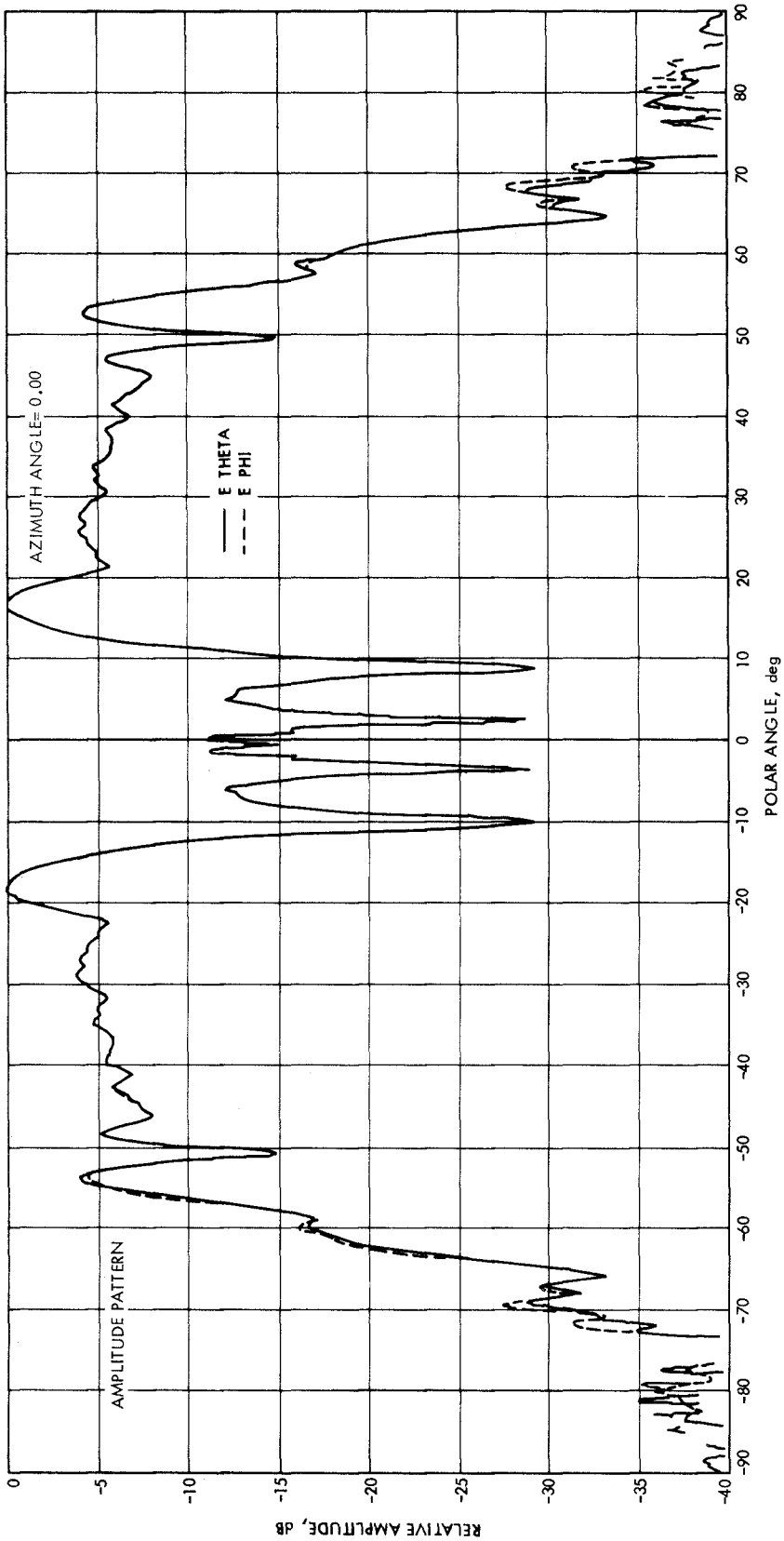

Fig. 8. The 22-dB standard horn at 8.5 GHz; Venus site hyperboloid with flange and vertex plate

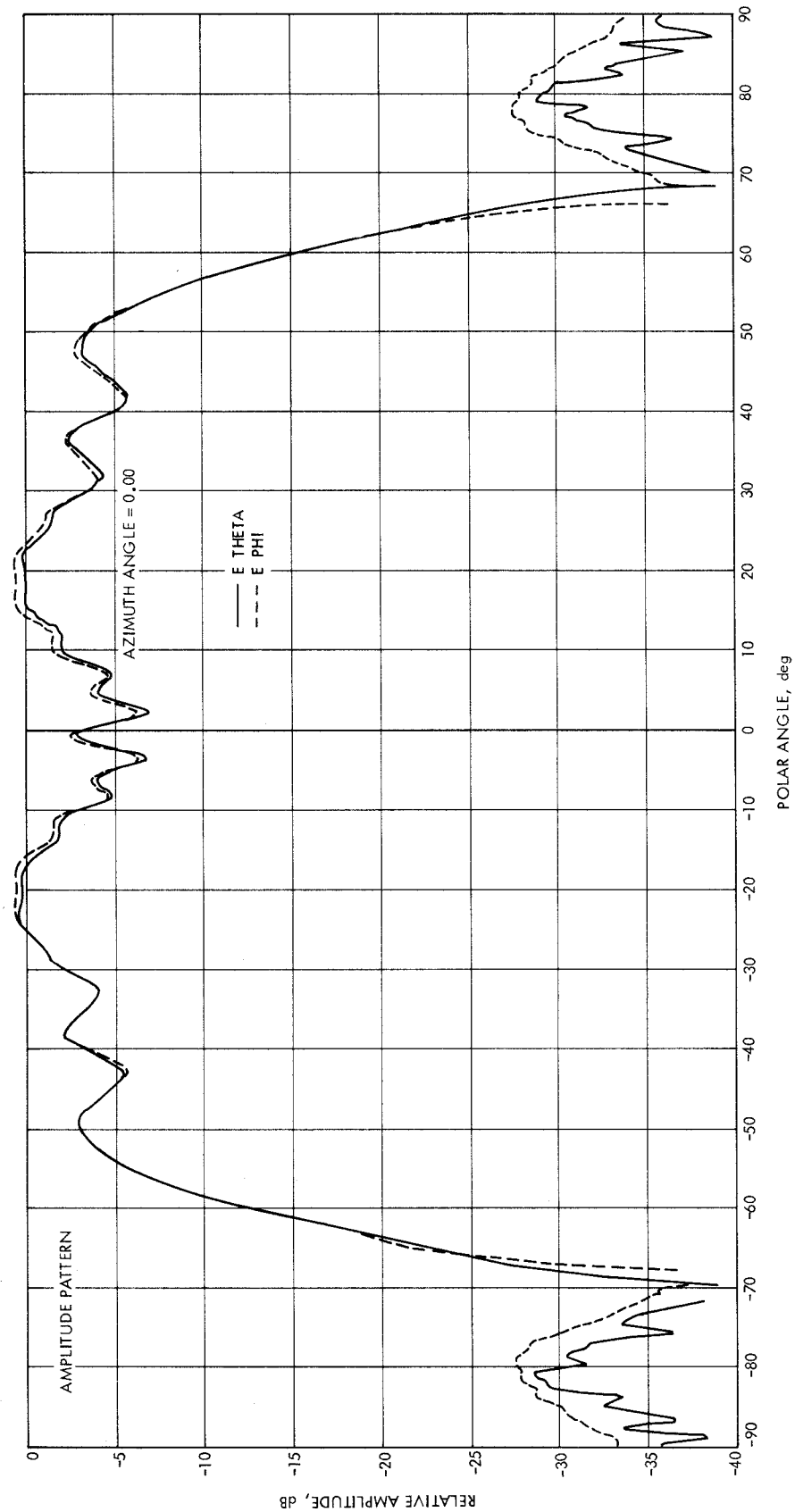

Fig. 9. The 17.1-deg horn at 4.6 (2.3) GHz; Venus site hyperboloid with flange and vertex plate

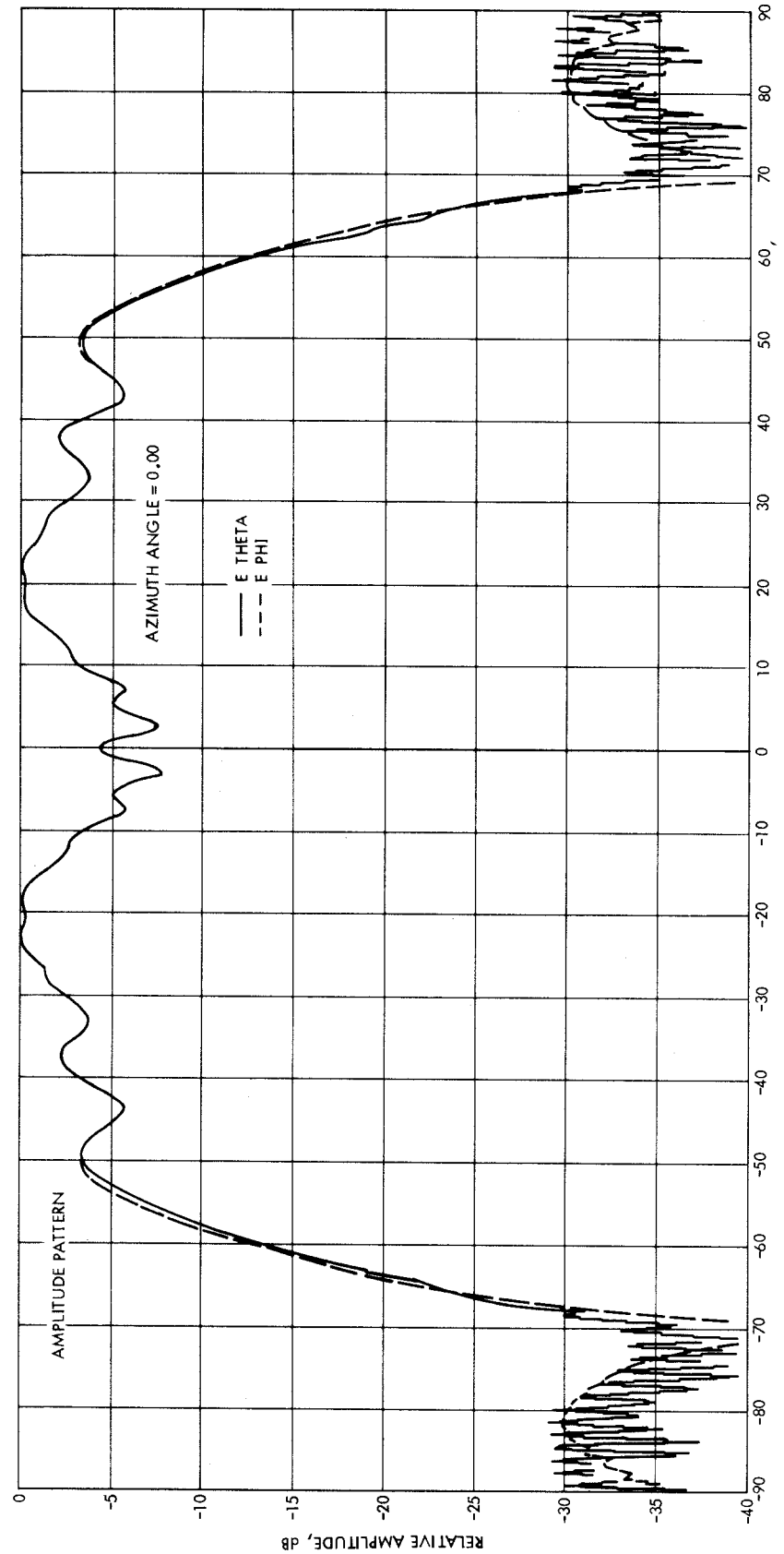

Fig. 10. The 22-dB standard horn at 2.3 GHz; Venus site hyperboloid with flange and vertex plate